New manifestations of $\chi^{(3)}$-nonlinear laser interactions in tetragonal $LuVO_4$ and $YbVO_4$ crystals attractive for SRS-converters and self-Raman lasers

2012 Laser Phys. Lett. 9 879

(http://iopscience.iop.org/1612-202X/9/12/008)

Abstract: We present several previously unexplored $\chi^{(3)}$-nonlinear laser effects under picosecond excitation in $LuVO_4$ and $YbVO_4$. Among them high-order Stokes and anti-Stokes generation related to discovered SRS-promoting vibration modes, with the manifestations of cross-cascaded $\chi^{(3)} \leftrightarrow \chi^{(3)}$ lasing processes involving new SRS-active phonons. All recorded spectral components of many-phonon $\chi^{(3)}$-nonlinear generation were identified and attributed to the vibrations of the $(VO_4)^{3-}$ structural units of the studied vanadates.

On the 50^{th} anniversary of the discovery of stimulated Raman scattering

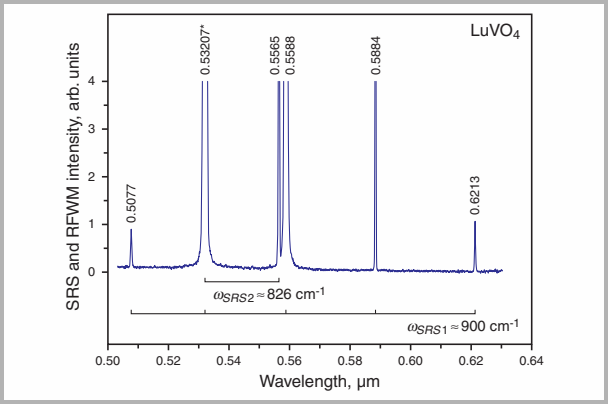

Selected part of a SRS and RFWM spectrum of a $LuVO_4$ single crystal recorded at room temperature with picosecond pumping at $\lambda_{f2} = 0.53207$ μm in excitation geometry $c(a,a)c$

New manifestations of $\chi^{(3)}$-nonlinear laser interactions in tetragonal $LuVO_4$ and $YbVO_4$ crystals attractive for SRS-converters and self-Raman lasers

A.A. Kaminskii, [1,*] *O. Lux,* [2,*] *H. Rhee,* [2] *H.J. Eichler,* [2] *K. Ueda,* [3] *H. Yoneda,* [3] *A. Shirakawa,* [3] *B. Zhao,* [4] *J. Chen,* [4] *J. Dong,* [5] *and J. Zhang* [6,7]

[1] Institute of Crystallography, Russian Academy of Sciences, Moscow 119333, Russia
[2] Institute of Optics and Atomic Physics, Technical University Berlin, 10623 Berlin, Germany
[3] Institute for Laser Science, University of Electro-Communications, Tokyo 182-8585, Japan
[4] College of Chemistry and Chemical Engineering, Fuzhou University, Fuzhou 350108, China
[5] Department of Electronic Engineering, School of Information and Technology of Xiamen University, Ximen 361005, China
[6] Jiangsu Normal University, Xuzhou 221116, China
[7] Nanyang Technological University, Singapore 639798, Singapore

Received: 16 April 2012, Revised: 28 June 2012, Accepted: 1 July 2012
Published online: 19 December 2012

Key words: centrosymmetric tetragonal crystal; $LuVO_4$; $YbVO_4$; stimulated Raman scattering; SRS; Stokes and anti-Stokes lasing; cross-cascaded $\chi^{(3)} \leftrightarrow \chi^{(3)}$ nonlinear generation

1. Introduction

After the discovery of high-gain stimulated Raman scattering (SRS) in the tetragonal vanadates YVO_4 and $GdVO_4$ in 2001 [1,2] and the prediction of their possible use in a $\chi^{(3)}$-laser, recent publications introduced two new SRS-active crystals of the $REVO_4$ (rare-earth vanadate) family – $LuVO_4$ [3] and $YbVO_4$ [4]. Subsequent pioneering works focused on the investigation of $\chi^{(3)}$-nonlinear laser interactions in the discovered SRS-active $REVO_4$ crystals, especially on the development of novel Raman converters such as self-Raman lasers with Ln^{3+}-dopants.

* Corresponding author: e-mail: kaminalex@mail.ru; oliver.lux@physik.tu-berlin.de

Crystal	SRS-promoting vibration modes, cm^{-1} [a]	Manifestations of $\chi^{(3)}$-nonlinear interactions [a]	Self-Raman lasers [b]
YVO_4	≈890, ≈838, ≈815 [1,2]	SRS, self-SFG(SRS) [c], THG(SRS) [d], $\chi^{(3)}$-cr-casc [e], $\chi^{(3)}$-comb [f]	Nd^{3+}($^4F_{3/2} \rightarrow {}^4I_{11/2}$ [6], $^4F_{3/2} \rightarrow {}^4I_{13/2}$ [7]); Yb^{3+}($^2F_{5/2} \rightarrow {}^2I_{7/2}$ [8])
$GdVO_4$	≈882, ≈807, ≈256 [1,2]	SRS, self-SFG(SRS) [c], THG(SRS) [d], $\chi^{(3)}$-cr-casc [e], $\chi^{(3)}$-comb [f]	Nd^{3+}($^4F_{3/2} \rightarrow {}^4I_{11/2}$ [5], $^4F_{3/2} \rightarrow {}^4I_{13/2}$ [9])
$YbVO_4$	≈897, ≈**823** [4]	SRS, self-SFG(SRS), THG(SRS), $\chi^{(3)}$-comb	
$LuVO_4$	≈900, ≈**826**, ≈**261**, ≈113 [3]	SRS, self-SFG(SRS), THG, $\chi^{(3)}$-cr-casc, $\chi^{(3)}$-comb	Nd^{3+}($^4F_{3/2} \rightarrow {}^4I_{11/2}$ [10])

[a] The results of this work are listed in bold letters.

[b] Only pioneering publications are listed here. In recent years, many types of self-Raman lasers have been developed on the basis of $REVO_4$ crystals doped with Nd^{3+} and Yb^{3+} ions (see e.g. [11–14] and their references).

[c] Self-SFG(SRS); the sum-frequency generation arising from SRS lasing Stokes and anti-Stokes components and pumping radiation.

[d] THG(SRS): the third harmonic generation by the parametric four-wave mixing (generation) with the participation of the pumping radiation at the fundamental wavelength (1.06415 μm) and its arising Stokes and anti-Stokes components.

[e] $\chi^{(3)}$-cr-casc: the cascade of one or many step $\chi^{(3)}$-lasing when in the photon-phonon generation of high-order Stokes and anti-Stokes components involved the interaction of different SRS-active promoting vibrational modes of the crystal.

[f] $\chi^{(3)}$-comb: the representation of the spectrum of Stokes and anti-Stokes laser frequency components with a width of at least one octave (the highest frequency (energy) component must be least double the lowest frequency component).

Table 1 Known SRS-active crystals of rare-earth orthovanadates with the tetragonal zircon-type structure

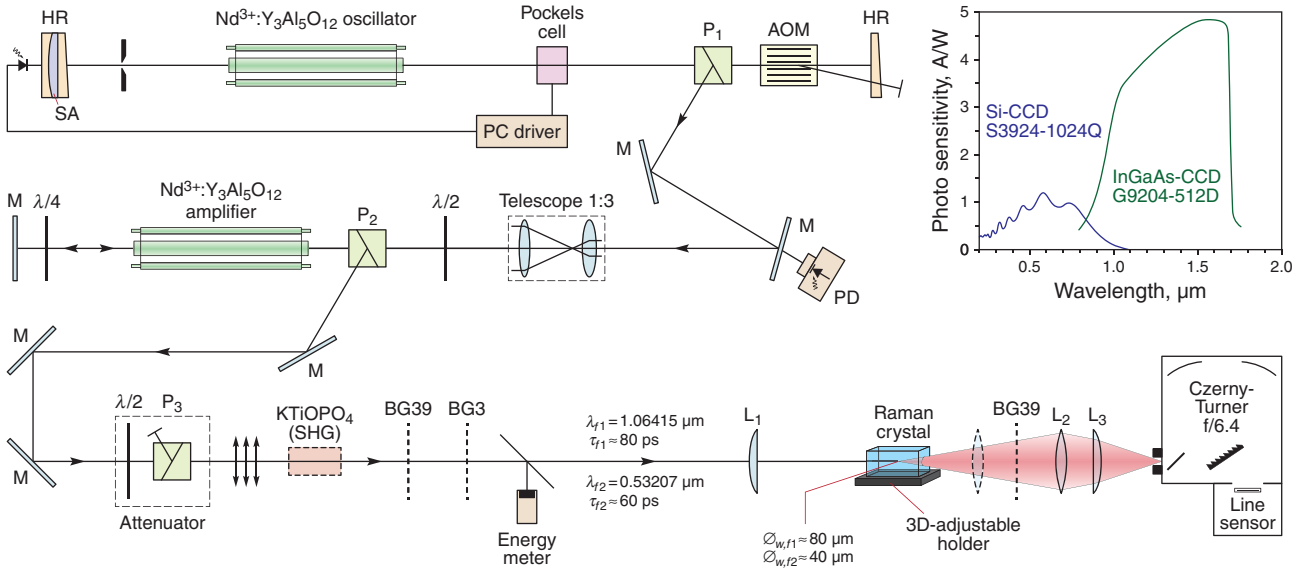

Figure 1 (online color at www.lasphys.com) Schematic diagram of the experimental setup. HR – resonator mirrors, SA – saturable absorber liquid, P_1 – P_3 – polarizers, AOM – acousto-optic modulator, M – mirrors, and L_1 – L_3 – lenses (see also text). The inset shows the spectral sensitivity of the employed Si- and InGaAs line sensors (data taken from Hamamatsu Photonics K.K. datasheet)

This research also motivated the analysis of the $\chi^{(3)}$-properties of other D_{4h}^{19}-tetragonal rare-earth vanadate crystals ($REVO_4$) of the zircon-type ($ZrSiO_4$) structures. Relatively soon, the experimental demonstration of such lasers has been carried out [5–8] (see Table 1). The research reported in this paper was performed in continuation of our previous SRS studies of $REVO_4$ crystals and is devoted to the results of investigations of new manifestations of $\chi^{(3)}$-nonlinear-laser interactions in $YbVO_4$ and $LuVO_4$ crystals.

2. Experimental setup

For the spectroscopic investigation of SRS and $\chi^{(3)}$-lasing photon-phonon interactions, we employed a hybridly mode-locked Xe-flashlamp pumped Nd^{3+}:$Y_3Al_5O_{12}$ laser in a master oscillator power amplifier (MOPA) setup as pump source (see Fig. 1). The stimulated emission wavelength of $\lambda_{f1} = 1.06415$ μm corresponds to the main laser inter-Stark transition 11507 cm^{-1} $^4F_{3/2} \rightarrow {}^4I_{11/2}$ 2110 cm^{-1} of the Nd^{3+}-ions [15]. This non-commercial

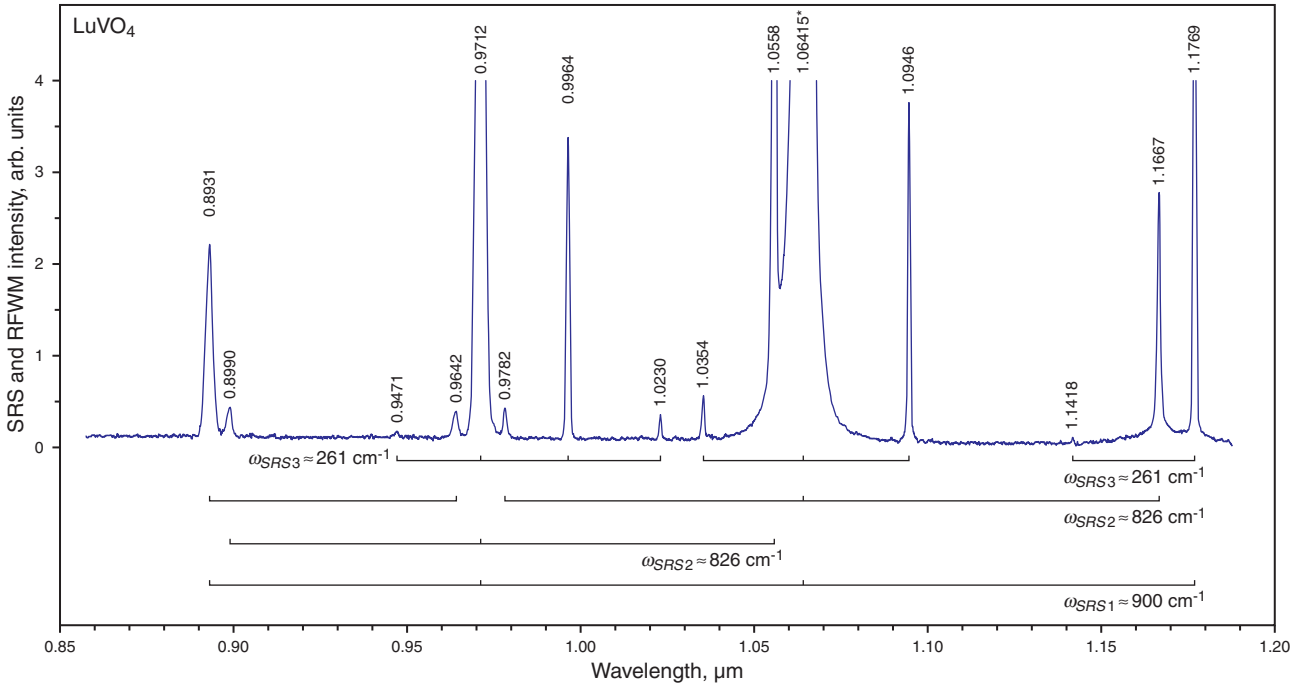

Figure 2 (online color at www.lasphys.com) Selected part of a SRS and RFWM spectrum of a $LuVO_4$ single crystal recorded at room temperature with picosecond pumping at $\lambda_{f1} = 1.06415$ μm in excitation geometry $c(ab, ab)c$. The wavelength of all lines (pump line is asterisked) is given in μm while the intensity is shown without correction for the spectral sensitivity of the used Si-CCD line sensor (its spectral sensitivity is shown in Fig. 1). Energy spacing (related to the SRS-promoting vibration modes $\omega_{SRS1} \approx 900$ cm^{-1}, $\omega_{SRS2} \approx 826$ cm^{-1}, and $\omega_{SRS3} \approx 261$ cm^{-1}) of the Stokes and anti-Stokes lasing sidebands are indicated by the horizontal scale brackets. The assignments of all recorded nonlinear-lasing lines are given in Table 2

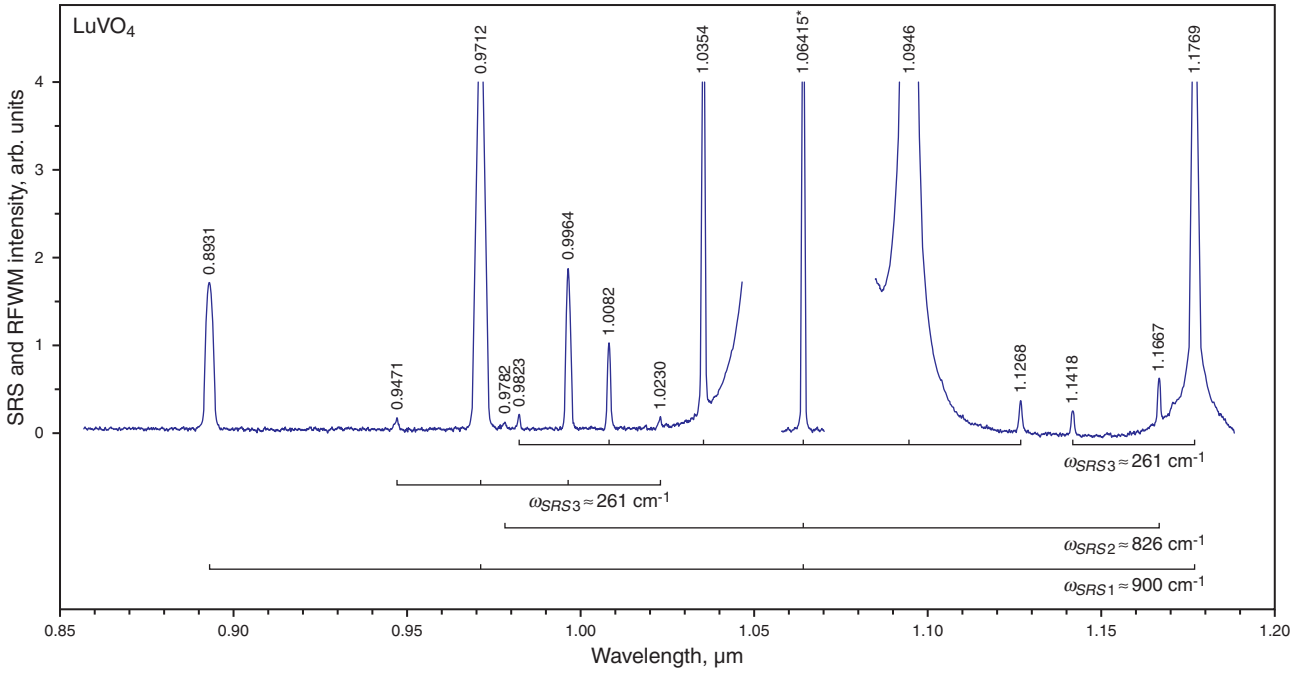

Figure 3 (online color at www.lasphys.com) Selected part of a SRS and RFWM spectrum of a $LuVO_4$ single crystal recorded at room temperature with picosecond pumping at $\lambda_{f1} = 1.06415$ μm in excitation geometry $c(\approx a, \approx a)c$. The used notations are analogous to that in Fig. 2

Excitation condition		Stokes and anti-Stokes $\chi^{(3)}$-generation			SRS-promoting vibration modes, cm^{-1}		
λ_f, μm	Pumping geometry [a]	Wavelength, μm [b]	Line [c]	Attribution of $\chi^{(3)}$-lasing components [d]	ω_{SRS1}	ω_{SRS2}	ω_{SRS3}
$LuVO_4$ crystal							
1.06415	$c(ab,ab)c$ (see Fig. 2)	0.8931	ASt_{2-1}	$*\omega_{f1}+2\omega_{SRS1}=\omega_{ASt2-1}$	≈900		
		0.8990	ASt_{1-2} ASt_{1-1}	$**\omega_{f1}+\omega_{SRS1}+\omega_{SRS2}=\omega_{ASt1-2,ASt1-1}$	≈900	≈826	
		0.9471	ASt_{1-3} ASt_{1-1}	$**\omega_{f1}+\omega_{SRS1}+\omega_{SRS3}=\omega_{ASt1-3,ASt1-1}$	≈900		≈261
		0.9642	St_{1-2} ASt_{2-1}	$**\omega_{f1}+2\omega_{SRS1}-\omega_{SRS2}=\omega_{St1-2,ASt2-1}$	≈900	≈826	
		0.9712	ASt_{1-1}	$*\omega_{f1}+\omega_{SRS1}=\omega_{ASt1-1}$	≈900		
		0.9782	ASt_{1-2}	$*\omega_{f1}+\omega_{SRS2}=\omega_{ASt1-2}$		≈826	
		0.9964	St_{1-3} ASt_{1-1}	$**\omega_{f1}+\omega_{SRS1}-\omega_{SRS3}=\omega_{St1-3,ASt1-1}$	≈900		≈261
		1.0230	St_{2-3} ASt_{1-1}	$**\omega_{f1}+\omega_{SRS1}-2\omega_{SRS3}=\omega_{St2-3,ASt1-1}$	≈900		≈261
		1.0354	ASt_{1-3}	$*\omega_{f1}+\omega_{SRS3}=\omega_{ASt1-3}$			≈261
		1.0558	St_{1-2} ASt_{1-1}	$**\omega_{f1}+\omega_{SRS1}-\omega_{SRS2}=\omega_{St1-2,ASt1-1}$	≈900	≈826	
		1.06415	λ_{f1}	ω_{f1}			
		1.0946	St_{1-3}	$\omega_{f1}-\omega_{SRS3}=\omega_{St1-3}$			≈261
		1.1418	ASt_{1-3} St_{1-1}	$**\omega_{f1}-\omega_{SRS1}+\omega_{SRS3}=\omega_{ASt1-3,St1-1}$	≈900		≈261
		1.1667	St_{1-2}	$\omega_{f1}-\omega_{SRS2}=\omega_{St1-2}$		≈826	
		1.1769	St_{1-1}	$\omega_{f1}-\omega_{SRS1}=\omega_{St1-1}$	≈900		
	$c(\approx a,\approx a)c$ (see Fig. 3)	0.8931	ASt_{2-1}	$*\omega_{f1}+2\omega_{SRS1}=\omega_{ASt2-1}$	≈900		
		0.9471	ASt_{1-3} ASt_{1-1}	$**\omega_{f1}+\omega_{SRS1}+\omega_{SRS3}=\omega_{ASt1-3,ASt1-1}$	≈900		≈261
		0.9712	ASt_{1-1}	$*\omega_{f1}+\omega_{SRS1}=\omega_{ASt1-1}$	≈900		
		0.9782	ASt_{1-2}	$*\omega_{f1}+\omega_{SRS2}=\omega_{ASt1-2}$		≈826	
		0.9823	ASt_{3-3}	$*\omega_{f1}+3\omega_{SRS3}=\omega_{ASt3-3}$			≈261
		0.9964	St_{1-3} ASt_{1-1}	$**\omega_{f1}+\omega_{SRS1}-\omega_{SRS3}=\omega_{St1-3,ASt1-1}$	≈900		≈261
		1.0082	St_{2-3}	$*\omega_{f1}+2\omega_{SRS3}=\omega_{St2-3}$			≈261
		1.0230	St_{2-3} ASt_{1-1}	$**\omega_{f1}+\omega_{SRS1}-2\omega_{SRS3}=\omega_{St2-3,ASt1-1}$	≈900		≈261
		1.0354	ASt_{1-3}	$*\omega_{f1}+\omega_{SRS3}=\omega_{ASt1-3}$			≈261
		1.06415	λ_{f1}	ω_{f1}			
		1.0946	St_{1-3}	$\omega_{f1}-\omega_{SRS3}=\omega_{St1-3}$			≈261
		1.1268	St_{2-3}	$*\omega_{f1}-2\omega_{SRS3}=\omega_{St2-3}$			≈261
		1.1418	ASt_{1-3} St_{1-1}	$**\omega_{f1}-\omega_{SRS1}+\omega_{SRS3}=\omega_{ASt1-3,St1-1}$	≈900		≈261
		1.1667	St_{1-2}	$\omega_{f1}-\omega_{SRS2}=\omega_{St1-2}$		≈826	
		1.1769	St_{1-1}	$\omega_{f1}-\omega_{SRS1}=\omega_{St1-1}$	≈900		
	$c(ab,ab)c$ (see Fig. 4a)	1.0354	ASt_{1-3}	$*\omega_{f1}+\omega_{SRS3}=\omega_{St1-3}$			≈261
		1.06415	λ_{f1}	ω_{f1}			
		1.0946	St_{1-3}	$\omega_{f1}-\omega_{SRS3}=\omega_{St1-3}$			≈261
		1.1096	ASt_{2-3} St_{1-1}	$**\omega_{f1}-\omega_{SRS1}+2\omega_{SRS3}=\omega_{ASt2-3,St1-1}$	≈900		≈261
		1.1268	St_{2-3}	$*\omega_{f1}-2\omega_{SRS3}=\omega_{St2-3}$			≈261
		1.1418	ASt_{1-3} St_{1-1}	$**\omega_{f1}-\omega_{SRS1}+\omega_{SRS3}=\omega_{ASt1-3,St1-1}$	≈900		≈261
		1.1667	St_{1-2}	$\omega_{f1}-\omega_{SRS2}=\omega_{St1-2}$		≈826	
		1.1769	St_{1-1}	$\omega_{f1}-\omega_{SRS1}=\omega_{St1-1}$	≈900		
		1.2142	St_{1-3} St_{1-1}	$**\omega_{f1}-\omega_{SRS1}-\omega_{SRS3}=\omega_{St1-3,St1-1}$	≈900		≈261
		1.2539	St_{2-3} St_{1-1}	$**\omega_{f1}-\omega_{SRS1}-2\omega_{SRS3}=\omega_{ASt2-3,St1-1}$	≈900		≈261
		1.2726	ASt_{1-3} St_{2-1}	$**\omega_{f1}-2\omega_{SRS1}+\omega_{SRS3}=\omega_{ASt1-3,St2-1}$	≈900		≈261
		1.3163	St_{2-1}	$*\omega_{f1}-2\omega_{SRS1}=\omega_{St2-1}$	≈900		
		1.3631	St_{1-3} St_{2-1}	$**\omega_{f1}-2\omega_{SRS1}-\omega_{SRS3}=\omega_{St1-3,St2-1}$	≈900		≈261
	$c(\approx a,\approx a)c$ (see Fig. 4b)	1.06415	λ_{f1}	ω_{f1}			
		1.0946	St_{1-3}	$\omega_{f1}-\omega_{SRS3}=\omega_{St1-3}$			≈261
		1.1418	ASt_{1-3} St_{1-1}	$**\omega_{f1}-\omega_{SRS1}+\omega_{SRS3}=\omega_{ASt1-3,St1-1}$	≈900		≈261
		1.1667	St_{1-2}	$\omega_{f1}-\omega_{SRS2}=\omega_{St1-2}$		≈826	

Excitation condition		Stokes and anti-Stokes $\chi^{(3)}$-generation			SRS-promoting vibration modes, cm^{-1}		
λ_f, μm	Pumping geometry [a]	Wavelength, μm [b]	Line [c]	Attribution of $\chi^{(3)}$-lasing components [d]	ω_{SRS1}	ω_{SRS2}	ω_{SRS3}
$LuVO_4$ crystal							
		1.1769	St_{1-1}	$\omega_{f1} - \omega_{SRS1} = \omega_{St1-1}$	≈900		
		1.1973	ASt_{1-2} St_{2-1}	$^{**}\omega_{f1} - 2\omega_{SRS1} + \omega_{SRS2} = \omega_{ASt1-2,St1-1}$	≈900	≈826	
		1.2142	St_{1-3} St_{1-1}	$^{**}\omega_{f1} - \omega_{SRS1} - \omega_{SRS3} = \omega_{St1-3,St1-1}$	≈900		≈261
		1.3036	St_{1-2} St_{1-1}	$^{**}\omega_{f1} - \omega_{SRS1} - \omega_{SRS2} = \omega_{St1-2,St1-1}$	≈900	≈826	
		1.3163	St_{2-1}	$^{*}\omega_{f1} - 2\omega_{SRS1} = \omega_{St2-1}$	≈900		
0.53207	$c(a,a)c$ (see Fig. 5)	0.5077	ASt_{1-1}	$^{*}\omega_{f2} + \omega_{SRS1} = \omega_{ASt1-1}$	≈900		
		0.53207	λ_{f2}	ω_{f2}			
		0.5565	St_{1-2}	$\omega_{f2} - \omega_{SRS2} = \omega_{St1-2}$		≈826	
		0.5588	St_{1-1}	$\omega_{f2} - \omega_{SRS1} = \omega_{St1-1}$	≈900		
		0.5884	St_{2-1}	$^{*}\omega_{f2} - 2\omega_{SRS1} = \omega_{St2-1}$	≈900		
		0.6213	St_{3-1}	$^{*}\omega_{f2} - 3\omega_{SRS1} = \omega_{St3-1}$	≈900		
$YbVO_4$ crystal							
0.53207	$c(a,a)c$ (see Fig. 6)	0.5078	ASt_{1-1}	$^{*}\omega_{f2} + \omega_{SRS1} = \omega_{ASt1-1}$	≈897		
		0.53207	λ_{f2}	ω_{f2}			
		0.5564	St_{1-2}	$\omega_{f2} - \omega_{SRS2} = \omega_{St1-2}$		≈823	
		0.5587	St_{1-1}	$\omega_{f2} - \omega_{SRS1} = \omega_{St1-1}$	≈897		
		0.5882	St_{2-1}	$^{*}\omega_{f2} - 2\omega_{SRS1} = \omega_{St2-1}$	≈897		
		0.6210	St_{3-1}	$^{*}\omega_{f2} - 3\omega_{SRS1} = \omega_{St3-1}$	≈897		

[a] Notations are used in analogy to [16]. The letters between parentheses are (from left to right) the polarization of the pumping and $\chi^{(3)}$-lasing scattering emission, respectively, while the ones to the left and the right of the parentheses are the pump and $\chi^{(3)}$-lasing scattering emission, respectively, In the case of $c(ab, ab)c$, the polarization direction for pump and scattered emission was directed between a and b axes.

[b] Measurement accuracy is ± 0.0003 μm.

[c] Here used notations: for example the notation St_{1-2} ASt_{1-1} is defined as the first Stokes component (related to the second SRS-promoting vibration mode $\omega_{SRS2} \approx 823$ cm^{-1}) generated from the first anti-Stokes emission (connected with the first SRS-active vibration mode $\omega_{SRS1} \approx 900$ cm^{-1}).

[d] The single- and double-asterisked lines mark the cascaded and cross-cascaded SRS and RFWM $\chi^{(3)}$-lasing processes, respectively. They are designated by the simplified notations for SRS and RFWM cascaded and cross-cascaded ($\chi^{(3)} \leftrightarrow \chi^{(3)}$)-lasing processes. The full designations of these processes should be, e.g. for the SRS cascade of the Stokes lasing: $\omega_{f1} + 3\omega_{SRS3} = (\omega_{f1} + \omega_{SRS3} + \omega_{SRS3} + \omega_{SRS3}) = \omega_{ASt3-3}$, and for the anti-Stokes lasing $\omega_{f1} + \omega_{SRS1} = \omega_{ASt1-1}$ it should contain four involved waves $\omega_{f1} + \omega_{SRS1} = [\omega_{f1} + \omega_{f1} - (\omega_{f1} - \omega_{SRS1})] = \omega_{f1} + \omega_{f1} - \omega_{St1-1} = \omega_{ASt1-1}$.

Table 2 Spectral composition of high-order cascaded and cross-cascaded Raman-induced Stokes and anti-Stokes $\chi^{(3)}$-nonlinear generation of orthorhombic crystals of $YbVO_4$ and $LuVO_4$, recorded at room temperature with picosecond Nd^{3+}:$Y_3Al_5O_{12}$-laser pumping at two fundamental wavelengths $\lambda_{f1} = 1.06415$ μm and $\lambda_{f2} = 0.53207$ μm

system uses an acousto-optic modulator (AOM) and a saturable absorber dye cell (SA) for active and passive mode-locking, respectively. A Glan-laser polarizer (P_1) linearly polarizes the laser emission at the plane of the optical table while a Pockels cell which is optically triggered by the leak radiation from the end mirror in the dye cell acts as a cavity dumper to obtain a single output pulse with about 1 mJ pulse energy and at 80 ps pulse duration.

After expansion of the beam diameter to 5.4 mm, a double-pass flashlamp pumped Nd^{3+}:$Y_3Al_5O_{12}$ amplifier is utilized to increase the single pulse energy up to 40 mJ to provide the intensities needed to efficiently excite $\chi^{(3)}$-lasing in the investigated orthovanadates. The amplified beam is then coupled out at a Glan-laser polarizer (P_2) and directed to the measuring part of the setup. Pulse energy variation is realized by a configuration consisting of a revolving half-wave-plate ($\lambda/2$) and a further Glan-laser polarizer (P_3), while the pump energy incident on the Raman-active crystal is monitored by measuring a small portion of the radiation with a pyroelectric energy meter (Polytec RjP-735). A spherical, plano-convex lens (L_1) with a focal length of 250 mm is used to focus the nearly Gaussian pump beam into the sample, resulting in a beam waist diameter of about 80 μm. The pump beam wavelength can be converted to $\lambda_{f2} = 0.53207$ μm by the second-harmonic generation (SHG) in a $KTiOPO_4$ (KTP) crystal with approximately 25% efficiency. This results in reduced pulse duration of 60 ps and a focus diameter of about 40 μm. A Schott BG39 filter glass with a transmission of 0.015% at 1.064 μm wavelength can be inserted behind the KTP

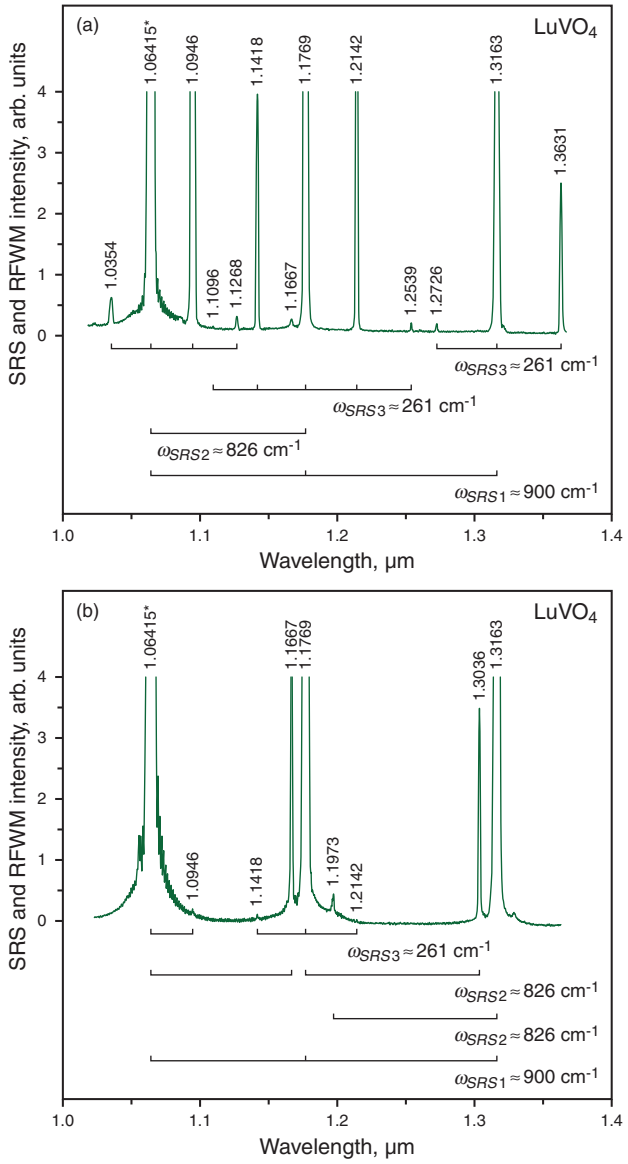

Figure 4 (online color at www.lasphys.com) Selected parts of SRS and RFWM spectra of a $LuVO_4$ single crystal recorded at room temperature with picosecond pumping at $\lambda_{f1} = 1.06415$ μm in excitation geometries: (a) $c(ab, ab)c$ and (b) $c(\approx a, \approx a)c$. The wavelength of all lines (pump lines are asterisked) are given in μm, the intensity is shown without correction for the spectral sensitivity of the used InGaAs line sensor (its spectral sensitivity is shown in Fig. 1). The used notations are analogous to that in Fig. 2

crystal to suppress the infrared component. Different excitation geometries can be adjusted by a customized crystalline sample stage with three translational and three rotational degrees of freedom. Due to the conical emission characteristics of Raman four-wave mixing (RFWM) and other nonlinear processes in the sample, it is necessary

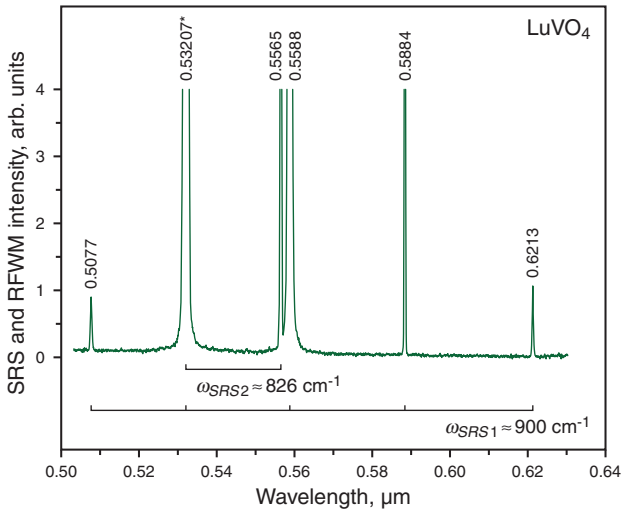

Figure 5 (online color at www.lasphys.com) Selected part of a SRS and RFWM spectrum of a $LuVO_4$ single crystal recorded at room temperature with picosecond pumping at $\lambda_{f2} = 0.53207$ μm in excitation geometry $c(a, a)c$. The wavelength of all lines (pump line is asterisked) are given in μm, the intensity is shown without correction for the spectral sensitivity of the used Si-CCD line sensor (its spectral sensitivity is shown in Fig. 1). Energy spacing (related to SRS-promoting vibration modes $\omega_{SRS1} \approx 900$ cm^{-1} and $\omega_{SRS2} \approx 826$ cm^{-1}) of the Stokes and anti-Stokes lasing sidebands are indicated by the horizontal scale brackets. The used notations are analogous to that in Fig. 2

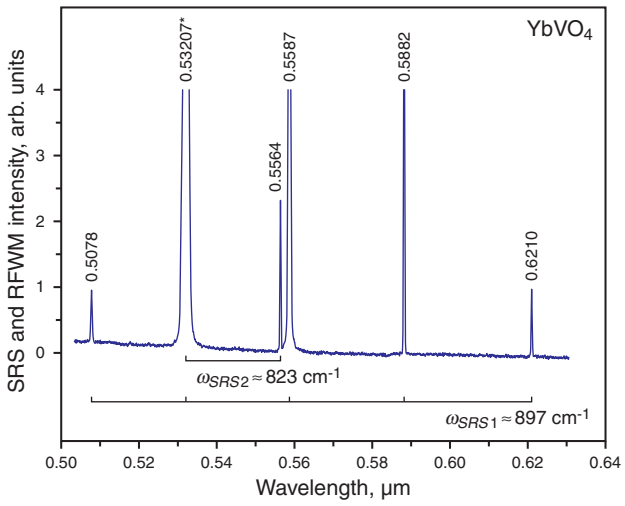

Figure 6 (online color at www.lasphys.com) Selected part of a SRS and RFWM spectrum of a $YbVO_4$ single crystal recorded at room temperature with picosecond pumping at $\lambda_{f2} = 0.53207$ μm in excitation geometry $c(a, a)c$. Energy spacing (related to SRS-promoting vibration modes $\omega_{SRS1} \approx 897$ cm^{-1} and $\omega_{SRS2} \approx 823$ cm^{-1}) of the Stokes and anti-Stokes lasing sidebands are indicated by the horizontal scale brackets. The used notations are analogous to that in Fig. 2 and Fig. 5

to exploit the complete acceptance angle of the grating spectrometer in Czerny-Turner arrangement used for signal detection (McPherson Model 270, 6.8 Å/pixel dispersion, 150 lines/mm grating). Therefore, a combination of a spherical bi-convex lens ($f_{L2} = 100$ mm) and a plano-convex cylindrical lens ($f_{L3} = 100$ mm) is utilized to image the divergent scattered emission onto the variable entrance slit of the spectrometer. An additional lens can be inserted behind the vanadate samples (in the form of rectangular bars with length of ≈ 20.4 mm for $LuVO_4$ and ≈ 6.4 mm for $YbVO_4$) for the detection of scattering components emitted in very large angles. The spectral composition of the radiation is finally recorded by a Si-CCD line sensor (Hamamatsu S3924-1024Q) for measurements in the UV and visible spectral region (see inset of Fig. 1). However, for near-IR spectra between 0.9 and 1.7 μm an InGaAs sensor was applied (Hamamatsu G9204-512D with 512 Pixels).

3. Nonlinear $\chi^{(3)}$-lasing in $YbVO_4$ and $LuVO_4$ crystals

Selected spectra of the performed measurements with tetragonal crystals of $YbVO_4$ and $LuVO_4$ and the results of their analysis are given in Fig. 2 – Fig. 6 and in Table 2. The given data conclusively evidences that – in comparison with our previous SRS-measurements – [3,4,17,18] we gained new knowledge about the nature of their $\chi^{(3)}$-nonlinear laser properties. This was possible due to a better optical quality of the used crystals as well as to improved pumping conditions with a modified experimental setup.

In particular, we were able to discover new $\chi^{(3)}$-promoting modes ($\omega_{SRS2} \approx 826$ cm^{-1} and $\omega_{SRS3} \approx 261$ cm^{-1} in $LuVO_4$ and $\omega_{SRS2} \approx 823$ cm^{-1} in $YbVO_4$). Furthermore, we observed cross-cascaded ($\chi^{(3)} \leftrightarrow \chi^{(3)}$) nonlinear lasing effects with the participation of two pairs of SRS-active $(VO_4)^{3-}$ molecular vibrations ($\omega_{SRS1} \approx 900$ cm^{-1} together with $\omega_{SRS2} \approx 826$ cm^{-1} and $\omega_{SRS1} \approx 900$ cm^{-1} together with $\omega_{SRS3} \approx 261$ cm^{-1}) in $LuVO_4$. These properties also manifested in almost all known SRS tetragonal $REVO_4$ vanadates (see Table 1).

The energy of their $\chi^{(3)}$-phonons as well as their steady-state Raman gain coefficients are very similar. In addition, they are able to generate octave-spanning Stokes and anti-Stokes lasing combs and while they all reliably exhibit up-conversion self-sum-frequency generation (self-SFG) processes, including the third harmonic generation (THG) under picosecond one-micron pumping.

The results of factor group analysis of spontaneous Raman scattering spectra of D_{4h}^{19}-tetragonal zircon-type $REVO_4$ crystals (with 12 atoms in the primitive cell ($Z^{Br} = 2$) and $3NZ^{Br} = 36$ degrees of freedom) testify about the identity of the nature of their 36 vibrational modes which relate to the irreducible representations (see, e.g. [19,20]): $\Gamma_{36} = 2A_{1g} + 4B_{1g} + B_{2g} + 5E_g + A_{2g} + B_{1u} + A_{1u} + B_{2u} + 4A_{2u} + 5E_u$. Among them, the first four species are Raman active modes. One of the recorded spontaneous Raman scattering spectra of the studied vanadates is shown in Fig. 7. It graphically explains the relationship of three components with vibrations of the tetrahedral $(VO_4)^{-3}$-ionic groups of the $LuVO_4$ crystal which lead to its many-phonons SRS lasing.

4. Conclusion

Obtained new data on the many-phonon SRS in $LuVO_4$ and $YbVO_4$ crystals (they are summarized in Table 2 and supplemented by Table 3 with some of their characteristics), greatly enriched our knowledge about the general processes occurring under steady-state $\chi^{(3)}$-nonlinear generation in the rare-earth vanadates ($REVO_4$) family with tetragonal zircon-type structure.

Some of these crystals (YVO_4, $GdVO_4$, and $LuVO_4$), doped with Ln^{3+}-ions (Nd^{3+} and Yb^{3+}) have been used for the development of self-Raman lasers. In order to achieve a more efficient operation of such lasers using these and other strong anisotropic $REVO_4$:Ln^{3+} vanadates, an extremely accurate adaption of their crystallographic orientation inside of the optical resonator with respect to the pump direction and under consideration of SE of the respective Ln^{3+}-lasants as well as of single-phonon SRS is required. We hope that the results of this work will help to address this important practical problem.

In conclusion, we note that within the framework of our further investigations we will continue to perform SRS experiments with other vanadates of this family of tetragonal crystals, including "mixed" crystals (solid solutions) such as $Lu_{0.5}Gd_{0.5}VO_4$, which is presently in the field of attention of laser researchers (see, e.g. [23,24] and its references).

Acknowledgements The authors wish to note that the investigations were considerably promoted through mutual scientific help within the "Joint Open Laboratory for Laser Crystals and Precise Laser Systems", and were stimulated by research programs of the Institute of Crystallography of the Russian Academy of Sciences, by the Institute of Optics and Atomic Physics of the Technical University of Berlin, by the Institute for Laser Science of the University of Electro-Communications. One of us (A.A.K) is grateful also to the Russian Foundation for Basic Research and to the Alexander von Humboldt Foundation.

References

[1] A.A. Kaminskii, K. Ueda, H.J. Eichler, Y. Kuwano, H. Kouta, S.N. Bagaev, T.H. Chyba, J.C. Barnes, G.M.A. Gad, T. Murai, and J. Lu, Opt. Commun. **194**, 201 (2001).
[2] A.A. Kaminskii, K. Ueda, H.J. Eichler, Y. Kuwano, H. Kouta, S.N. Bagayev, T.H. Chyba, J.C. Barnes, T. Murai, and J. Lu, Laser Phys. **11**, 1124 (2001).

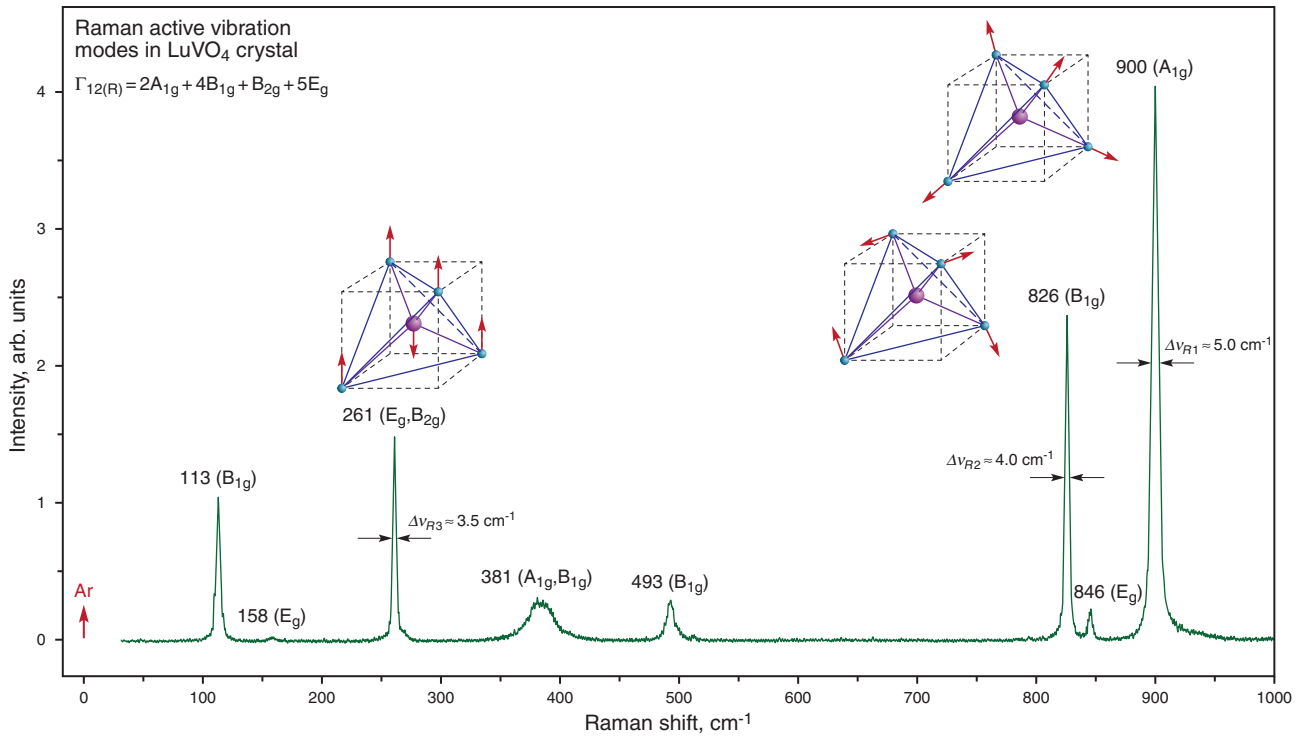

Figure 7 (online color at www.lasphys.com) Room-temperature polarized spontaneous Raman scattering spectrum for the tetragonal $LuVO_4$ single crystal under Ar-ion laser excitation at 0.488 μm wavelength (shown by the arrow). The Raman shifted lines are given in cm^{-1} with an indication of the symmetry of vibration modes (in parentheses). The full width at half maximum (FWHM) linewidths are indicated only for the lines related to SRS-promoting internal vibration modes of the crystal recorded in the present work. The insets show the displacement of the atoms in the tetrahedral $(VO_4)^{3-}$ ionic groups for the three SRS-active modes [19]

Characteristics [a]	**$LuVO_4$**	**$YbVO_4$**
Space group	$D_{4h}^{19} - I4_1/amd$ (No. 141)	
Unit-cell parameters, Å	$a=b=7.026$, $c=6.234$	$a=b=7.1192$, $c=6.2898$
X-ray density, g cm^{-3}	$d_x \approx 6.233$	$d_x \approx 6.12$
Melting temperature, °C	≈ 1800	
Method of crystal growth	Czochralski; floating zone; flux	
Linear optical classification	Positive ($n_o < n_e$) uniaxial	
Nonlinearity	$\chi^{(3)}$	
Optical transparency range, μm	$\approx 0.3 - \approx 5.5$	$\approx 0.33 - \approx 5.2$
Thermal conductivity, W/m/K	$\kappa_{\parallel a}=7.896$, $\kappa_{\parallel c}=9.414$	$\kappa_{\parallel a} \approx 5.1$, $\kappa_{\parallel c} \approx 3.9$ [100]
Energy of the SRS-promoting vibration mode, cm^{-1}	$\omega_{SRS1} \approx 900$, $\omega_{SRS2} \approx 826$, $\omega_{SRS3} \approx 261$, $\omega_{SRS4} \approx 113$	$\omega_{SRS1} \approx 897$, $\omega_{SRS2} \approx 823$
Steady-state Raman gain coefficient for the first Stokes lasing related to the ω_{SRS1} with picosecond pumping at 1.06415 μm wavelength, cm/GW	$g_{ssR}^{St_{1-1}} \geq 3.2$	$g_{ssR}^{St_{1-1}} \geq 2.9$ [b]
Lasing Ln^{3+}-ions [c]	Nd^{3+}, Tm^{3+}, Yb^{3+}	–

[a] See corresponding references in [7,8].

[b] The steady-state Raman gain coefficients for the first Stokes lasing were measured in [21] to be 17.8±0.2 cm/GW under pimping at 0.532 μm wavelength (SHG of Nd^{3+}:$Y_3Al_5O_{12}$ picosecond laser) and 29±0.2 cm/GW under THG-wavelength pumping at 0.355 μm.

[c] At present, from these two vanadates only $LuVO_4$ is used as the host-crystal for Ln^{3+}-lasant ions (see, e.g. [22]).

Table 3 Room-temperature crystallographic and some selected physical properties of SRS-active tetragonal vanadates $LuVO_4$ and $YbVO_4$

[3] A.A. Kaminskii, H. Rhee, H.J. Eichler, K. Ueda, K. Oka, and H. Shibata, Appl. Phys. B **93**, 865 (2008).
[4] A.A. Kaminskii, H.J. Eichler, H. Rhee, K. Ueda, K. Oka, and H. Shibata, Laser Phys. **18**, 1546 (2008).
[5] T.T. Basiev, S.V. Vassiliev, V.A. Konjushkin, V.V. Osiko, A.I. Zagumennyi, Y.D. Zavartsev, S.A. Kutovoi, and I.A. Shcherbakov, Laser Phys. Lett. **1**, 237 (2004).
[6] Y.F. Chen, Opt. Lett. **29**, 1915 (2004).
[7] Y.F. Chen, Opt. Lett. **29**, 2172 (2004).
[8] Y.F. Chen, Opt. Lett. **29**, 2632 (2004).
[9] V.E. Kisel, A.E. Troshin, N.A. Tolstik, V.G. Shcherbitsky, N.V. Kuleshov, V.N. Matrosov, T.A. Matrosova, and M.I. Kupchenko, Appl. Phys. B **80**, 471 (2005).
[10] A.A. Kaminskii, M. Bettinelli, J. Dong, D. Jaque, and K. Ueda, Laser Phys. Lett. **6**, 374 (2009).
[11] Y.T. Chang, H.L. Chang, K.W. Su, and Y.F. Chen, Opt. Express **17**, 11892 (2009).
[12] T. Omatsu, A. Lee, H.M. Pask, and J. Piper, Appl. Phys. B **97**, 799 (2009).
[13] Y.F. Lü, W.B. Cheng, Z. Xiong, J. Lu, L.J. Xu, G.C. Sun, and Z.M. Zhao, Laser Phys. Lett. **7**, 787 (2010).
[14] Y.M. Duan, G. Zhang, Y.J. Zhang, Q.L. Jin, H.Y. Wang, and H.Y. Zhu, Laser Phys. **21**, 1859 (2011).
[15] A.A. Kaminskii, Sov. Phys. JETP **24**, 33 (1967); A.A. Kaminskii, Laser Crystals, Their Physics and Properties (Springer, Berlin, 1980 and 1990).
[16] T.C. Damen, S.P.S. Porto, and B. Tell, Phys. Rev. **142**, 570 (1966).
[17] A.A. Kaminskii, S.N. Bagayev, K. Oka, H. Shibata, K. Ueda, K. Takaichi, H.J. Eichler, and H. Rhee, Laser Phys. Lett. **3**, 263 (2006).
[18] A.A. Kaminskii, S.N. Bagayev, H.J. Eichler, H. Rhee, K. Ueda, K. Takaichi, K. Oka, H. Shibata, Y. Hatanaka, and Y. Matsumoto, Laser Phys. Lett. **3**, 385 (2006).
[19] S.A. Miller, H.H. Caspers, and H.E. Rast, Phys. Rev. **168**, 964 (1968).
[20] C.C. Santos, E.N. Silva, A.P. Ayala, I. Guedes, P.S. Pizani, C.-K. Loong, and L.A. Boatner, J. Appl. Phys. **101**, 053511 (2007).
[21] D.W. Hu, Z.P.Wang, H.J. Zhang, X.G. Xu, J.Y. Wang, and Z.S. Shao, Acta Phys. Sinica **57**, 1704 (2008), in Chinese.
[22] A.A. Kaminskii, Laser Photon. Rev. **1**, 93 (2007).
[23] H.H. Yu, H.J. Zhang, Z.P. Wang, J.Y. Wang, Y.G. Yu, D.Y. Tang, G.Q. Xie, H. Luo, and M.H. Jiang, Opt. Express **17**, 3264 (2009).
[24] A.A. Kaminskii, O. Lux, H. Rhee, H.J. Eichler, H. Yoneda, A. Shirakawa, K. Ueda, B. Zhao, J. Chen, J. Dong, and J. Zhang, Appl. Phys. B **109**, 649 (2012).